



Article

Landslide Susceptibility Prediction Using GIS, Analytical Hierarchy Process, and Artificial Neural Network in North-Western Tunisia

Manel Mersni ^{1,*}, Dhekra Souissi ², Adnen Amiri ¹, Abdelaziz Sebei ³ , Mohamed Hédi Inoubli ¹ and Hans-Balder Havenith ⁴ 

¹ Unité de Recherche de la Géophysique Appliquée aux Minerais et Matériaux (URGAMM), Faculté des Sciences de Tunis, Université Tunis El Manar, Tunis 2092, Tunisia; adnen.amiri@fst.utm.tn (A.A.); mohamedhedi.inoubli@fst.utm.tn (M.H.I.)

² Laboratoire des Interactions Plantes, Sols et Environnements LR21ES01, Faculté des Sciences de Tunis, Université Tunis El Manar, Tunis 2092, Tunisia; dhekra.souissi@fst.utm.tn

³ Laboratoire des Ressources Minérales et Environnement LR01ES06, Faculté des Sciences de Tunis, Université de Tunis El Manar, Tunis 2092, Tunisia; abdelaziz.sebei@fst.utm.tn

⁴ Laboratoire de Géorisques et Environnement, Département de Géologie, Université de Liège, 4000 Liège, Belgium; hb.havenith@uliege.be

* Correspondence: manel.mersni@etudiant-fst.utm.tn; Tel.: +216-22-632366

Abstract

Landslide susceptibility modelling represents an efficient approach to enhance disaster management and mitigation strategies. The focus of this paper lies in the development of a landslide susceptibility evaluation in northwestern Tunisia using the Analytical Hierarchy Process (AHP) and Artificial Neural Network (ANN) approaches. The used database covers 286 landslides, including ten landslide factor maps: rainfall, slope, aspect, topographic roughness index, lithology, land use and land cover, distance from streams, drainage density, lineament density, and distance from roads. The AHP and ANN approaches were applied to classify the factors by analyzing the correlation relationship between landslide distribution and the significance of associated factors. The Landslide Susceptibility Index result reveals five susceptible zones organized from very low to very high risk, where the zones with the highest risks are associated with the combination of extreme amounts of rainfall and steep slope. The performance of the models was confirmed utilizing the area under the Relative Operating Characteristic (ROC) curves. The computed ROC curve (AUC) values (0.720 for ANN and 0.651 for AHP) convey the advantage of the ANN method compared to the AHP method. The overlay of the landslide inventory data locations of historical landslides and susceptibility maps shows the concordance of the results, which is in favor of the established model reliability.

Keywords: landslide susceptibility mapping; GIS; AHP; ANN; histogram method; ROC curve



Academic Editor: Ioannis Koukouvelas

Received: 6 May 2025

Revised: 13 July 2025

Accepted: 22 July 2025

Published: 3 August 2025

Citation: Mersni, M.; Souissi, D.; Amiri, A.; Sebei, A.; Inoubli, M.H.; Havenith, H.-B. Landslide Susceptibility Prediction Using GIS, Analytical Hierarchy Process, and Artificial Neural Network in North-Western Tunisia. *Geosciences* **2025**, *15*, 297. <https://doi.org/10.3390/geosciences15080297>

Copyright: © 2025 by the authors. Licensee MDPI, Basel, Switzerland. This article is an open access article distributed under the terms and conditions of the Creative Commons Attribution (CC BY) license (<https://creativecommons.org/licenses/by/4.0/>).

1. Introduction

Landslides have become a global topic of study due to the growing knowledge of their socioeconomic effects and the urbanization pressures on mountain zones [1]. A recent bibliometric analysis [2] reveals a consistent increase in annual publications from 8 in 1982 to 2432 in 2020. Landslides are recognized as among the most prevalent geohazards in mountainous regions [3,4] that can be influenced by a number of natural and

manufactured causes [5]. The landslide consequences include fatalities and significant damage to infrastructure [6]. During the period of 2004 to 2016, 4862 landslide events were reported worldwide, resulting in 55,000 fatalities [7,8]. The effects of landslides can be devastating not only on human lives but also on the economy. The Emergency events show that landslides have caused more than 2.7 USD [9]. In Tunisia, the Northwestern part is recognized as highly vulnerable to landslides. For instance, in February 2012, after a heavy rainfall and snowfall, the Ain Draham region experienced a considerable number of landslides, reaching a total of 120 incidents affecting 98 individuals causing the breakdown of the bridge connecting Hammam Bourguiba and Ain Draham and the obstruction of the primary roadways providing access to the town with any financial repercussions of this incident amount to 35 million dinars [10].

Thus, mitigation and identification of landslide risk remain a challenging task for local government and decision-makers. In order to achieve this, landslide susceptibility mapping is an efficient approach for management and mitigating risks through identifying the landslide susceptible zone [11,12]. Various approaches can be used to ensure the evaluation of landslide susceptibility, specifically AHP [13–15], frequency ratio Fr [16,17]. Recently, machine learning has become a popular trend among researchers; it is commonly employed in geohazard susceptibility mapping, particularly for landslides [18–20], such as ANN [21–23], decision trees DT [24,25], support vector machines SVM [26,27], random forest RF [28,29], adaptive neuro-fuzzy inference system ANFIS [30,31], and logistic regression [32,33]. Numerous researchers have proposed methods to mitigate uncertainty, which involve combining predictions from multiple algorithms [34–36].

Limited studies have been conducted in northern Tunisia to map landslide susceptibilities; each study used a different method to assess landslide susceptibility in specific geographic areas within northern Tunisia. Ref. [37] utilized the evidential belief functions (EBF) and weight of evidence (WoE) models to generate landslide susceptibility maps for northwestern Tunisia. Ref. [38] employed the fuzzy gamma operator and GIS to assess landslide susceptibility along a section of national road No. 11, from Mateur to Béja. Ref. [39] employed the frequency ratio (FR) and statistical index (SI) models to create sensitivity maps for landslides. Ref. [40] utilized fuzzy logic to develop a landslide susceptibility map for Mogods and Hedil. There is no study that has used ML to create a map of landslide susceptibility.

The present study employed the AHP and ANN to assess landslide susceptibility on the northwestern part of Tunisia and identify the area's most at-risk. The landslide locations were meticulously inventoried and represented as polygons. This inventory was informed by reports of past landslides, data series obtained from Google Earth, and expert opinions, complemented by extensive field surveys. Ten factors were selected for consideration, as per the previous research, a questionnaire survey, and the availability of relevant data, including rainfall, slope, aspect, TRI, lithology, LULC, distance from streams, drainage density, lineament density, and distance from roads.

TanDEM-X, the most current, most accurate, and extensive global DEM datasets of the Earth surface [41], was the one we used to derive five landslide factors due to its availability. The accuracy of landslide susceptibility mapping is influenced by the source of the dataset that was used for DEMs as per [42,43]. According to previous studies [43], using high-resolution DEMs like TanDEM-X 12m instead of lower resolution DEMs significantly improves the performance of landslide susceptibility mapping. After production of the completed landslide inventory map and subsequent choice of relevant parameters, landslide susceptibility modelling is implemented to determine areas at risk of landslides and predict where such events are most likely to happen. By using the

outcomes of the two models, this study can help regional planners choose effective models for predicting landslides in the northwest of Tunisia.

2. Materials and Methods

2.1. Study Area

The research zone (Figure 1) is part of the Kroumirie mountain range, in the northwest of Tunisia. It extends over an area of approximately 983.335 km². It is bounded in the north by the Mediterranean Sea and the Fernana delegation in the south, Beja to the east, and to the west by Algeria. Due to the steep slopes, heavy precipitation, and lithostratigraphic series, mainly composed of clay, as well as anthropogenic factors, Landslide hazards represent a significant risk to the concerned area. This zone is known for its mountainous terrain, with elevations varying from sea level to 1238 m, decreasing significantly from southwest to northeast and south to north. The regional climate of the research area is Mediterranean. The average amount of rainfall per year from 2000 to 2020 is between 964.84 and 1747.81 mm (the Regional Commissariat for Agricultural Development of Jendouba). This area receives significant rainfall, which supports the formation of a dense network of streams and rivers. The study area's vegetation is widely regarded as being extensive, occupying 39.7% of the land.

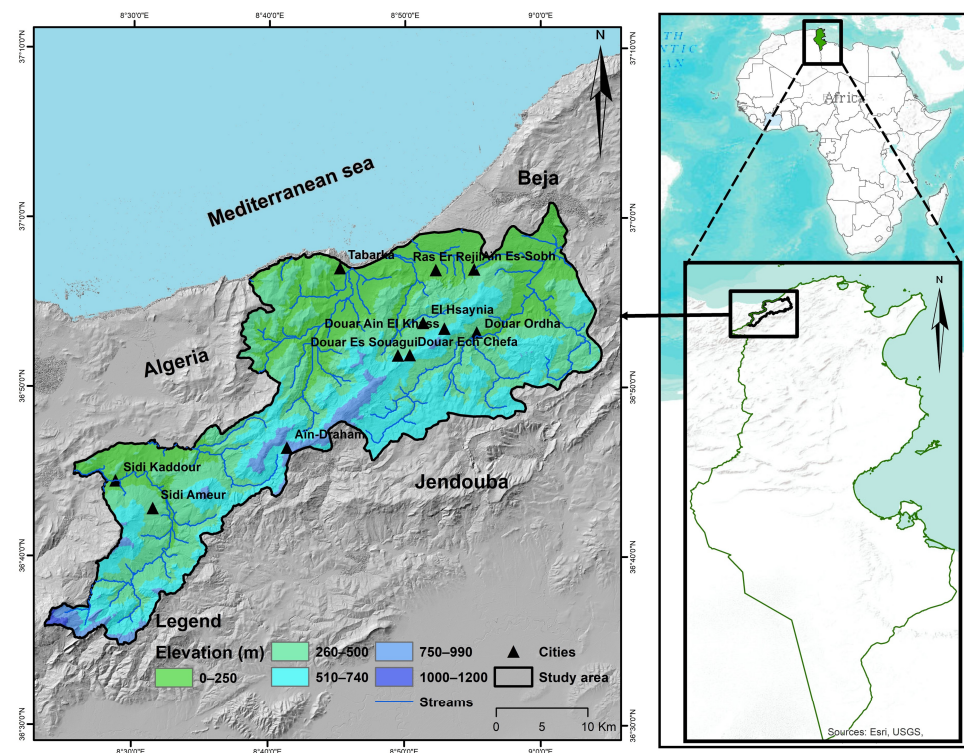


Figure 1. Study area map showing the elevation and the rivers with a hill-shaded map.

Geologically, the research area is situated in the nappe zone (Tellian zone) and consists mainly of allochthonous terrains. These terrains, ranging in age from Triassic to Neogene, have been displaced from their original locations due to significant tectonic movements [44] (Figure 2). The area is dominated by clay interspersed with limestone, marl, and sandstone deposits. This area is notably affected by folds and overlaps, predominantly oriented in the NE-SW direction. The north-east to south-west orientation of the tectonic features correlates with the geographical distribution of seismic events in the area.

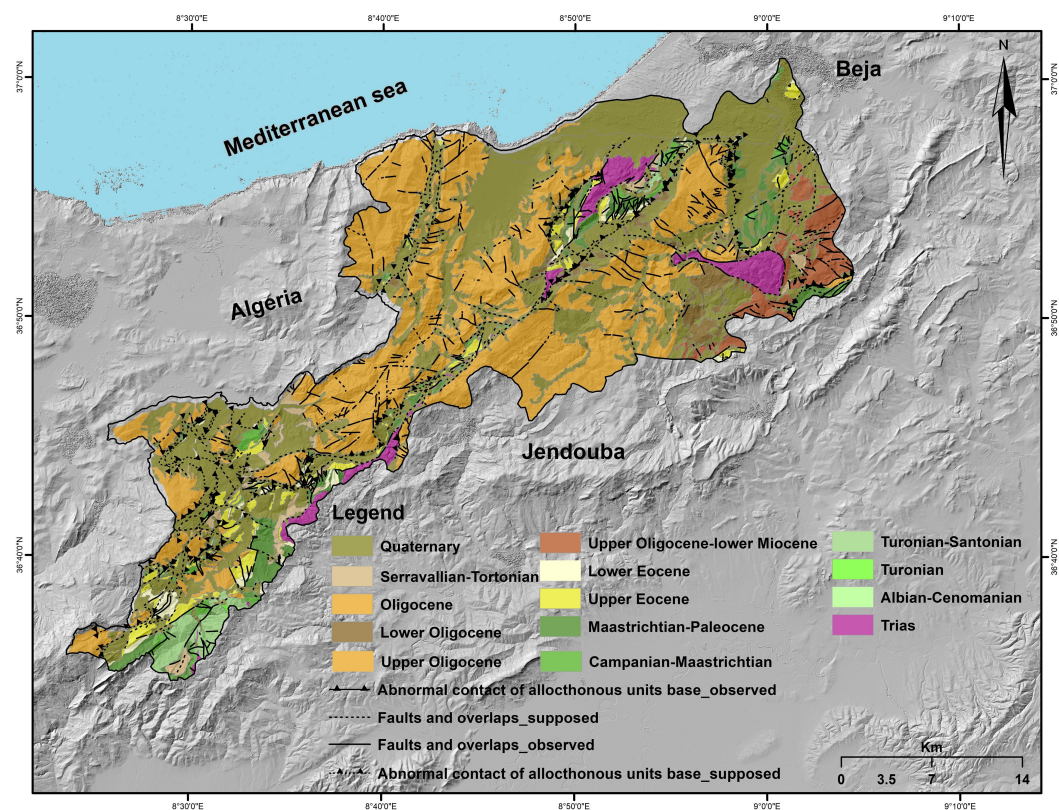


Figure 2. Geological map of the study area.

2.2. Input Data

The present research involved the establishment of a spatial database within a Geographic Information System (GIS) environment, encompassing a map of inventory, ten landslide factor maps (Table 1).

Table 1. Input data used and derived landslide factors.

Input Data Type	Reference	Derivative Maps
Landslide location	Historical records, Google Earth, and previous studies	Landslide inventory map
TanDEM-X DEM 12m	The German Aerospace Center (DLR)	Maps of slope, aspect, TRI, distance from streams, drainage density
Sentinel 2A	The Copernicus Scientific Hub (https://scihub.copernicus.eu/dhus accessed on 1 October 2023)	LULC map Lineament density map
Geological map (5 maps) five geological maps 1/50.000	National Office of Mines (NOM)	Lithology map
Roads data	Open street map	Distance from roads map
Meteorological data	Regional Commissariat for Agricultural Development of Jendouba (RCADJ)	Rainfall map

2.2.1. Landslide Inventory Map

The northwestern part of Tunisia has been historically affected by several landslides, specifically in 2012 after an extensive rainfall and snowfall, most of which occurred at the level of the national road N° 17. In the current study, the inventory map of landslides (Figure 3) is created through a series of field surveys conducted between 2020 and 2024, as well as historical landslide reports from the Ministry of Equipment’s archives and Google

Earth data from 2004 to 2024. This research does not classify landslides because information on their type is not available.

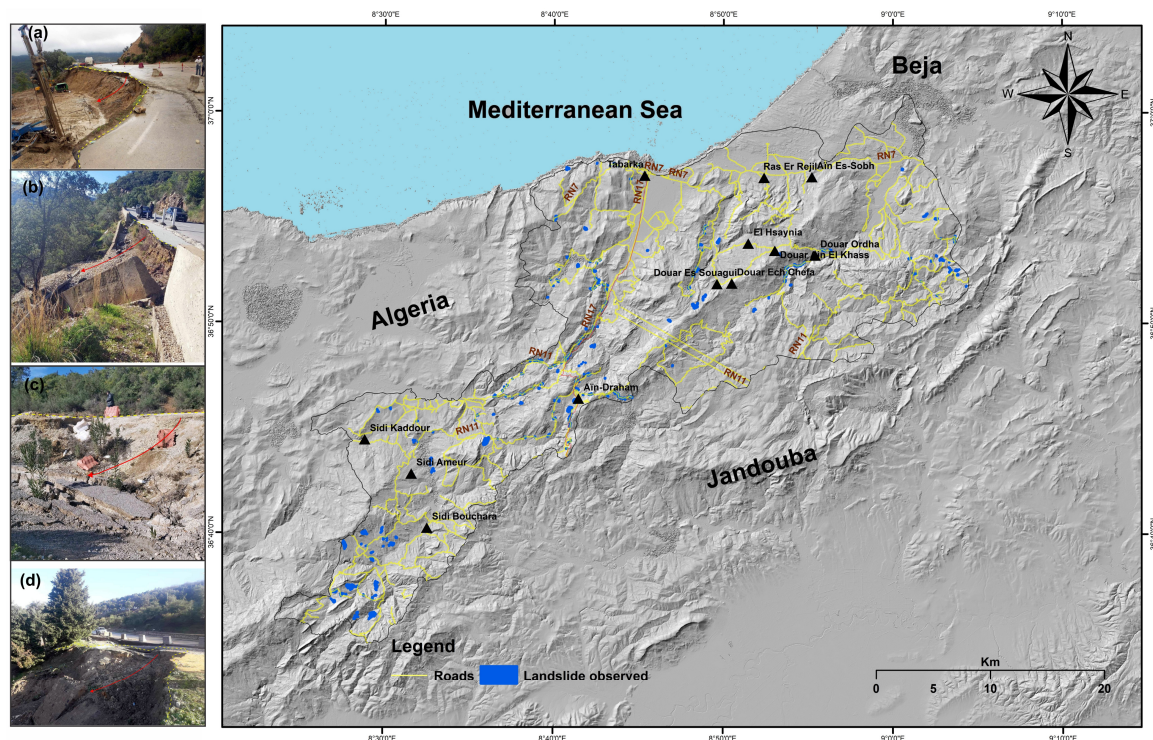


Figure 3. The inventory map of the landslides in the study area. Photos clearly show the damage caused by the landslide. The red arrow designates the slope movement direction. (a) Landslide on the national road RN_17 (2015); (b) landslide of Ain Jmal on the national road RN_17 (2019); (c) landslide of Ain Sbaa in the regional road RR 161 (2019); (d) landslide of Ain Boumerchane on the national road RN_17 (2018).

2.2.2. Landslide Factors

To accurately assess the susceptibility of landslides, it is necessary to select the appropriate and most influential factors [45,46]. Hence, in the present study, ten landslide factors, rainfall, slope, aspect, TRI, lithology, LULC, distance from streams, drainage density, lineament density, and distance from roads, were selected based on the questionnaire survey, the data availability, and previous research.

Rainfall

Rainfall plays a crucial role in causing landslides because it raises groundwater levels and pore water pressure [22]. Furthermore, as rain infiltrates, shear strength weakens and friction between the soil and bedrock decreases, which can lead to a landslide hazard [47]. Many studies [48,49] have examined correlations between landslide events and rainfall. Rainfall data were gathered from the Jandouba Regional Commissariat for Agricultural Development. The average annual rainfall for 20 years, from 2001 to 2021, of ten rain gauge stations (Ain Draham, Ain El Khass, Ain Soboh, Dar Echeffa, Hammam Bourguiba Barrage, Majen Essef, Oued Zeen, Tabarka AER, Ain Debba, Ain Hamraya) was calculated, then a rainfall map was produced utilizing the ID interpolation approach in the tool in ArcGIS. The research area's rainfall map indicates a range of rainfall from 970 to 1700 mm annually (Figure 4a).

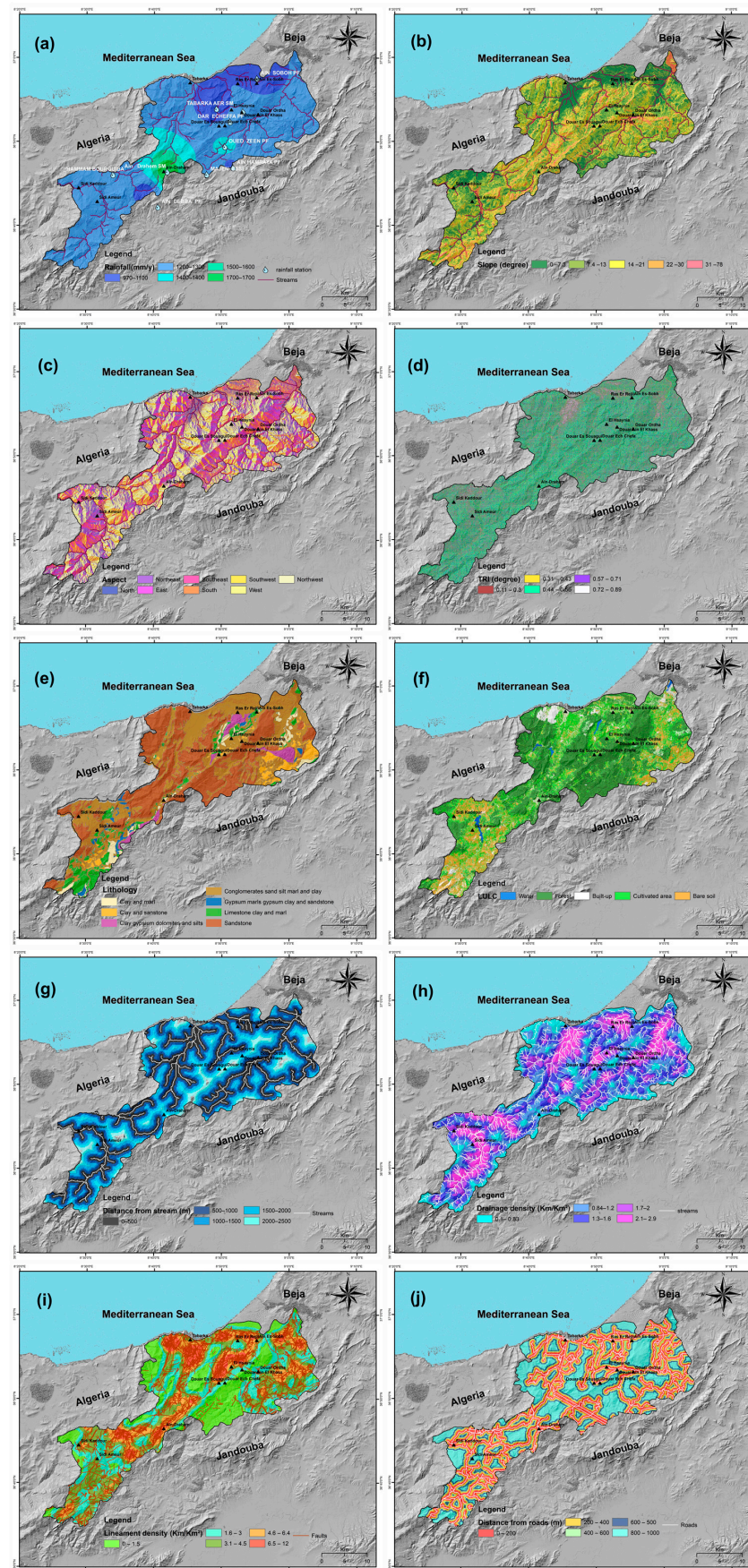


Figure 4. Landslide factors maps employed in the present study. (a) Rainfall, (b) slope, (c) aspect, (d) TRI, (e) lithology, (f) LULC, (g) distance from streams, (h) drainage density, (i) lineament density, (j) distance from roads.

Slope

Slope is recognized as one of the most significant and fundamental factors for evaluating landslide susceptibility because it is responsible for controlling the shear forces acting on hill slopes [50,51]. According to several studies [52,53], landslides are more likely to occur when the slope increases. The slope map is derived from TanDEM-X 12m with five defined categories (Figure 4b).

Aspect

Aspect refers to the slope direction, which is one of the parameters used to map the susceptibility of landslides [19,54]; it affects the landslide processes indirectly by influencing evapotranspiration, sunlight duration, humidity, moisture, and the types and distribution of vegetation cover [55]. The TanDEM-X DEM 12m is used to produce the aspect map through the Aspect function in the ArcGIS software (version 10.8). The aspect was classified into eight orientations (Figure 4c).

Topographic Roughness Index (TRI)

TRI determines the elevation differences between a central cell in a digital elevation model (DEM) and its surrounding cells. Recently, TRI has been frequently adopted in a number of landslide susceptibility research studies [18,56]. According to [57], the areas affected by landslides are often very rugged. Furthermore, ref. [58] observed high roughness values on the surfaces of landslides. In the present research, the TRI is extracted from the DEM using QGIS and ArcGIS software. It is subdivided into five classes (Figure 4d).

Lithology

Lithology impacts landslides through its properties, such as the permeability, porosity, and the strength of the rock or the soil [53,56]. Different types of lithology display varying levels of susceptibility to potential sliding and subsequent failure [59]. For instance, the study of [60] concluded that claystone is a significant factor in the formation of landslides. The lithological map of the current research area is compiled using five geological maps (Tabarka, Ain Drahem, Fernana, Bou Salem, and Zahret Madyen) on a 1/50,000 scale, which were created by the National Office of Mines (NOM). These maps were assembled, georectified, and digitized. The study area includes the following lithological types: Clay and marl, Clay and sandstone, Clay gypsum dolomites and silts, Conglomerates, sand silt marl and clay, Gypsum marls gypsum clay and sandstone, Limestone clay and marl, Sandstone (Figure 4e).

Land Use Land Cover (LULC)

Slope stability could be enhanced by the hydrological and mechanical effects of vegetation [55,61,62]. Areas characterized by low vegetation cover experience greater susceptibility to slope failure than forested areas [63]. The Sentinel 2A obtained from the Copernicus Scientific Hub is processed to generate the map of LULC by utilizing the Maximum Likelihood Method of Classification in ArcGIS. Five land use classes were defined for the study area, including forest, water area, built-up, cultivated area, and bare soil, as shown in Figure 4f.

Distance from streams

The proximity of rivers and streams plays a crucial role in controlling landslides, as evidenced by many studies [52,62]. Stability can be negatively impacted by streams through erosion and excessive moisture content in slope materials [61,64]. It is noted by [61,65] that the number of landslides decreases as the distance from the stream increases. Landslide occurrences are more likely to happen in areas located near rivers, especially in mountainous regions. In this research, the distance from streams map was created employing the Buffer tool in ArcGIS. Five buffer zones are categorized as depicted in Figure 4g.

Drainage density

Drainage density is defined as the total length of all drainage channel segments per unit area. It is the cause of landslides [45,66]. According to studies [66,67], high drainage density can lead to the development of channels and gullies that serve as pathways for debris to move downward. Hence, a high drainage density can be a sign of areas that are potentially landslide-prone. For this research, the drainage density map was made with the use of the line density tool in ArcGIS software (Figure 4h).

Lineament density

Lineament density represents geological structures such as zones of weakness, discontinuities, shear zones, faults, and fractures [68]. It has been proven by research [69] that regions characterized by a dense lineament network are more susceptible to increased weathering and partial landslides that involve unstable lithologies, while those with low to medium lineament density are less likely to face more stable rocks and fewer landslides. The lineament density map was obtained from Sentinel-A2 imagery utilizing the software tools mentioned (SNAP, Envi, Geomatica, and ArcGIS). The produced lineament density map was subsequently categorized into five distinct categories, as illustrated in Figure 4i.

Distance from roads

Distance from roads, as an anthropogenic factor, is taken into account in the susceptibility mapping of landslides and has been incorporated in numerous research findings [22,23]. The presence of roads in mountainous areas can result in an increased frequency of landslides, as stated by researchers [63,70], because the development of roads changes the topography of the area [71]. Areas in close proximity to roads tend to be more susceptible to landslides than those situated at a greater distance because building roads involves cutting into the slopes, which can affect their stability [72]. In the current study, the distance from the road map was determined by employing the Euclidean distance method in the ArcGIS software. Five classes are categorized to indicate the impact of proximity to roads on landslide occurrence, as depicted in Figure 4j.

2.3. Method

2.3.1. Background of the Method

The adopted methodology (Figure 5) involves the selection of ten influencing criteria of the landslide risk in the study area, including rainfall (RF), slope (SL), aspect (AS), TRI, lithology (LG), LULC, distance from streams (DS), drainage density (DD), lineament density (LD) and distance from roads (DR).

The final susceptibility maps consisted of the following steps: First, after the weighting calculation, ten raster layers were prepared in the ArcGIS environment. These landslide factors were derived from a variety of sources, each of which had a different resolution. In order to achieve data standardization, the raster layers were subsequently resampled [73,74] using the Resample tool in ArcGIS. This tool is used to resize the raster. The resampled raster layers were reclassified to ensure they were all using the same scale. The Raster Calculator tool in ArcGIS was consequently used to input the raster layers. The rasters were then multiplied by their respective weights and summed. Finally, the landslide susceptibility map has been reclassified as follows: very low, low, moderate, high, and very high susceptibility classes.

These landslide factors are ranked in order of importance according to the Saati scale. For the AHP method, the importance of the range of landslide factors is based on a questionnaire survey that was addressed to the authorities—Expert opinion (Regional Department of Equipment and Infrastructure of Jendouba, Protection Civil, Municipal Office, and Local Department of Forestry). In order to identify the landslide risk zone, a spatial analysis (GIS-MCDM) and statistical modelling, AHP and ANN were applied. The use of such models has been increasing recently as a reliable alternative to on-site exploration. Indeed, the

GIS-based MCDM-AHP-ANN method is a valuable approach for enhancing land surface assessment. It provides a comprehensive spatiotemporal distribution of observations at a large scale, saving time and money. Two prediction models were applied to determine the weights of landslide factors. The main adopted prediction methods include the prediction of landslide susceptibility prototype using the ANN and AHP models. These latter are utilized to derive the weights of the landslide factors.

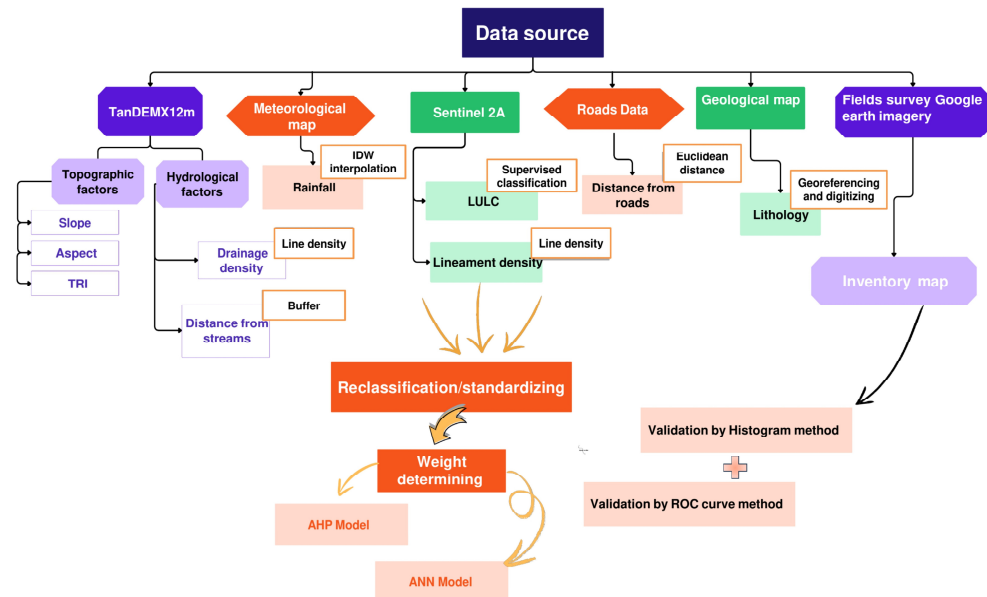


Figure 5. Adopted methodology Flowchart.

2.3.2. Weightage Calculation

Multiple influencing factors have been identified to delimit the potential landslide risk areas. The weight of each relationship is determined by its importance in the landslide susceptibility potential (LLS_{pot}). A weighting of 0.5 and 1.0 was attributed, respectively, to the minor and major factor [69–71]. The relative rates are calculated considering the cumulative weightage of both minor and major effects. Then, this relative rate is utilized in order to determine the score of each landslide factor by using Equation (1).

$$\text{Score} = ((M + m)) / \sum (M + m) \times 100 \quad (1)$$

where M: major inter-relationship between two parameters. m: Minor inter-relationship between two parameters.

2.3.3. Analytical Hierarchy Process (AHP)

The AHP model is a decision support system that employs a multi-criteria and multi-objective approach to facilitate optimal resolution of complex problems [75]. It achieves this by evaluating and ranking multiple alternatives using pair-wise comparisons. Statistical theory is a theory of measurement used to create weight scales from pairwise comparisons [76]. The pairwise-comparison matrix method (PWC-AHP) is established by [77] as part of the analytic hierarchy process. The purpose of this method of analysis involves the identification of the relative importance of selected factors in achieving a stated goal. The initial step in the AHP method consists of the creation of a pair-wise comparison matrix (PCM-AHP) [78]. This matrix shows the relative importance of one factor compared to the others, based on the decisions of makers. This technique is measured employing a Saaty scale with the following levels of significance: 3 = moderately, 5 = strongly, 7 = very

strongly, 9 = extremely, and 2, 4, 6, 8 = intermediate values. Weights from 1 to $9\frac{1}{9}$ were assigned for the less important variables. The diagonal criteria are equal to (2).

$$W \text{ (PCM-AHP)} = \begin{bmatrix} 1 & w_{12} & \dots & w_{1n} \\ \frac{1}{w_{12}} & 1 & \dots & \frac{1}{w_{2n}} \\ \vdots & \vdots & \ddots & \vdots \\ \frac{1}{w_{1n}} & \frac{1}{w_{2n}} & \dots & 1 \end{bmatrix} \quad (2)$$

The normalization and relative weighting of parameters can be computed in order to calculate the relative impact of the conditional factors.

$$\sum_{i=1}^n w_i w_i(x, y) = 1 \quad (3)$$

The Pairwise Comparison Matrix's results are employed to normalize the eigenvector elements (w) associated with the λ_{\max} (maximum eigenvalue) [79–81].

$$n\lambda_{\max} = \sum_{k=1}^n \left(\sum_{j=1}^n \varepsilon_{kj} \right) = \sum_{i=1}^n \varepsilon_{ii} + \sum_{\substack{i,j=1 \\ i \neq j}}^n (\varepsilon_{ji} + \varepsilon_{ij}) = n + \sum_{\substack{i,j=1 \\ i \neq j}}^n (\varepsilon_{ji} + \varepsilon_{ij}^{-1}) \geq n + \frac{n^2 - n}{2} = n^2 \quad (4)$$

$$MnW = \lambda_{\max} \times W \quad (5)$$

To ensure consistency in the calculated weights from PWC-AHP, it is necessary that (CR) is lower than 0.1. Inconsistencies are possible if the Consistency Ratio (CR) value exceeds 0.1. It is therefore necessary to revise the pairwise matrix.

$$\mu = \frac{\lambda_{\max} - n}{n - 1}, \quad \lambda_{\max} = \sum \left(\left(\sum n_j \right) \times \left(\sum n_i \right) \right) \quad (6)$$

$$CR = CI/RI \quad (7)$$

Finally, the local ratings of each parameter were determined by multiplying the rating by the weights of the various classes of each factor.

2.3.4. Artificial Neural Network (ANN)

An ANN is a machine-learning model [56]. This computer program is capable of acquiring, organizing, presenting, calculating, and developing maps from a variety of multivariate geospatial data. It uses a non-linear transfer process to deliver these maps [82].

As illustrated in Equation (8), from a mathematical perspective, a neuron can be defined as follows [23]:

$$y = \phi \left(\sum_{j=1}^n w_j x_j + b \right) \quad (8)$$

The output signal of the neuron is denoted by y , while the input signals are indicated by x_1, \dots, x_n . The weights are denoted by w_1, \dots, w_n , and the bias is denoted by b . Finally, the activation function is denoted by ϕ .

The aim of the artificial neural network (ANN) model is to develop a system capable of predicting results from input factors not utilized in the modelling procedure [82]. The back-propagation learning algorithm is the most common method for neural networks [82]. The neural network (NN) structure includes three layers (Figure 6), an input layer relative to landslide conditional criteria, a hidden layer, and an output layer associated with the landslide susceptibility model. To train the neural network, the resilient backpropagation with weight backtracking algorithm uses the relationship established between historical landslide events and potential causative parameters (Table 2).

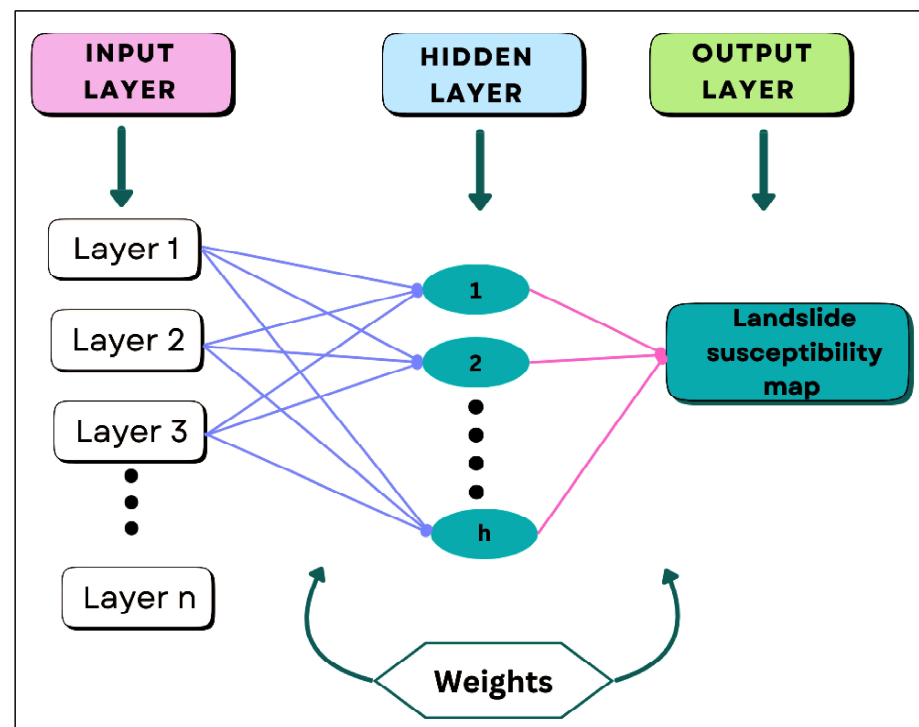


Figure 6. Architecture of the Artificial Neural Networks model used for landslide susceptibility modelling.

Table 2. Hyperparameter settings of the ANN model [83–85].

Machine Learning Method	Hyperparameter	Range
ANN	Algorithm	Backprop, RPROP+, RPROP-, SLR, SAG, GRPROP
	Activation function	[TanH, Relu, Logistic]
	Optimization method	[SGD, Adam, Nadam, Adamax, Adadelata, Adagrad, RMSprop]
	Neurons in hidden layers	one hidden layer with three neurons
	Layer	3
	Batch size	(4, 128)
	Momentum coefficient	(0.5, 1)

In this study, the landslide inventory data are represented in a binary (0, 1) format, where ‘0’ represents non-landslide pixels and ‘1’ designates landslide pixels. The ‘N’ package focuses on MLP, which is well applicable in modeling functional relationships.

ANNs learn complex process interrelationships of a system independently, and they can be applied to the problem of slip surface detection even when the exact relationship is little understood [52]. To produce a trustworthy ANN prototype that predicts reliable surface positions, true field data must be used.

2.3.5. Model Validation

Validation is the crucial step for modelling [23]. The ROC curve is the most popular method to validate the efficiency of landslide susceptibility prototypes [86–88]. The performance of landslide susceptibility prototypes is assessed based on the reliability of the ROC curve tests [89]. The area under the curve (AUC) value provides a quantitative measure

to compare model performance. An AUC value approaching 100% indicates an increase in the reliability of the model. If the AUC equals 50%, the model is unable to distinguish between landslides and non-landslides [21]. In the current study, the performance of the generated landslide susceptibility models was tested through the use of the ROC curve and the susceptibility area histogram method, which involves overlaying historical landslide locations on landslide maps.

3. Results

The revealed results of the ANN and AHP models (Table 3) express the importance of the rainfall and slope factors. These latter are defined as the highest weight, followed by aspect, TRI, lithology, and LULC, respectively. The other factors are considered less important.

Table 3. Weights of landslide factors computed by ANN and AHP models.

Factor	AHP	ANN	Classes	Reclassify	Description of the Landslide Potential
Rainfall (mm/y)	22.37	23.96	970–1100	1	Very low
			1200–1300	2	Low
			1400–1400	3	Moderate
			1500–1600	4	High
			1700–1700	5	Very high
Slope (%)	22.37	23.96	0–7.3	1	Very low
			7.4–13	2	Low
			14–21	3	Moderate
			22–30	4	High
			31–78	5	Very high
Aspect	13.07	14.02	North	1	Very low
			Northeast	3	Moderate
			East	3	Moderate
			Southeast	5	Very high
			South	4	High
			Southwest	3	Moderate
			West	3	Moderate
TRI (%)	13.07	14.02	Northwest	2	Low
			0.11–0.3	1	Very low
			0.31–0.43	2	Low
			0.44–0.56	3	Moderate
			0.57–0.71	4	High
Lithology	8.34	7.39	0.72–0.89	5	Very high
			Clay and marl	5	Very high
			Clay and sandstone	4	High
			Clay gypsum dolomites and silts	5	Very high
			Conglomerates sand silt marl and clay	2	Low
			Gypsum marls clay and sandstone	4	High
			Limestone clay and marl	3	Moderate
			Sandstone	1	Very low

Table 3. Cont.

Factor	AHP	ANN	Classes	Reclassify	Description of the Landslide Potential
LULC	6.12	5.13	Water area	5	Very high
			Forest	1	Very low
			Built up	2	Low
			Cultivated area	4	High
			Bare soil	5	Very high
Distance from Streams (m)	4.57	3.715	0–500	5	Very High
			500–1000	4	High
			1000–1500	3	Moderate
			1500–2000	2	Low
			2000–2500	1	Very low
Drainage density (km/km ²)	3.59	3.715	0.1–0.83	1	Very low
			0.84–1.2	2	Low
			1.3–1.6	3	Moderate
			1.7–2	4	High
			2.1–2.9	5	Very high
Lineament density (km/km ²)	3.25	2.045	0–1.5	1	Very low
			1.6–3	2	Low
			3.1–4.5	3	Moderate
			4.6–6.4	4	High
			6.5–12	5	Very high
Distance from roads (m)	3.25	2.045	0–200	5	Very high
			200–400	4	High
			400–600	3	Moderate
			600–800	2	Low
			800–1000	1	Very low

As illustrated in Figure 7a, highly susceptible areas to landslides coincide with significant rainfall intensity over 1500 mm annually. Landslides are more prone to occur during periods of increased precipitation intensity. In addition, areas with steep slopes, spatially the class (31–78°), are more prone to landslides (Figure 7b). The southeast and south aspect classes convey the highest susceptibility to landslide, followed by the east and northeast direction (Figure 7c). The lithological layers characterized by the dominance of clay facies are more susceptible to landslides (Figure 7e) and contribute to slope instability. Referring to LULC, landslides are most likely to occur in the bare soil and water categories, followed by the cultivated area, and the forest category is least likely to experience them (Figure 7f). Considering distance from streams and distance from roads, the nearest streams and roads increase the potential for landslides (Figure 7g,j).

Regions exhibiting high to very high drainage density (over 1.3 to 1.6 km/km²) are correlated with an increase in landslide occurrences (Figure 7h). This is explained by the link between surface runoff and soil saturation. For lineament density, areas marked by a density of lineaments around (3.1–4.5 km/km² to 4.6–6.4 km/km²) are more exposed to landslides (Figure 7i). TRI values between 0.31–0.43° and 0.44–0.56° are associated with the landslide risk zones (Figure 7d).

Landslide susceptibility distribution of the north-west of Tunisia was established based on ANN and AHP methods. The models of landslide susceptibility are divided into five susceptibility zones according to the natural break method: very low, low, moderate, high, and very high (Figure 8). As shown in the landslide susceptibility maps (Figure 8a,b), there are substantial differences in the areas covered by the susceptible zones.

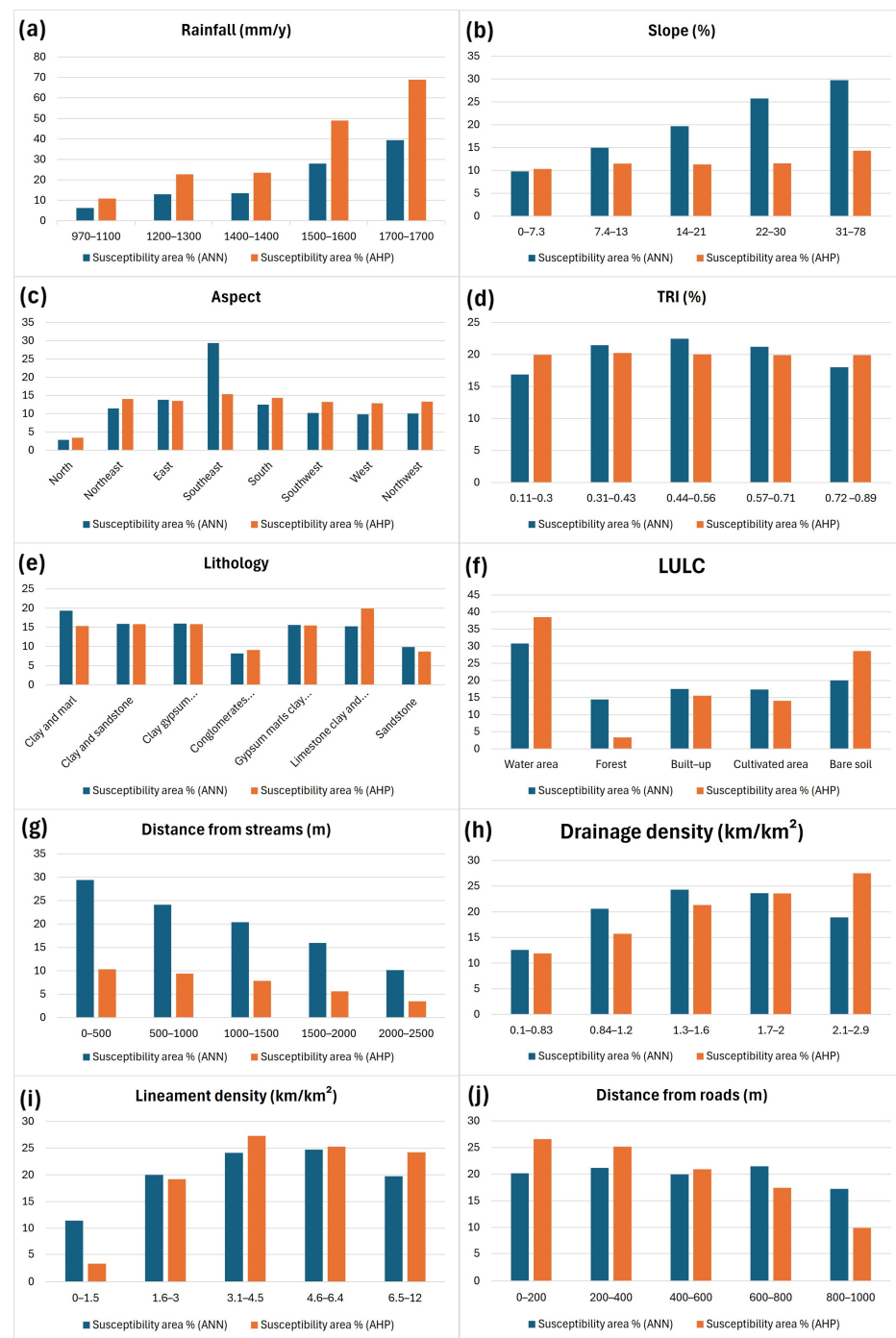


Figure 7. Relationships between susceptible (high to very high) regions and classes of landslide factors. (a) Rainfall, (b) slope, (c) aspect, (d) TRI, (e) lithology, (f) LULC, (g) distance from streams, (h) drainage density, (i) lineament density, (j) distance from roads.

The landslide susceptibility maps evidence that the center of the research area, including the cities of Ain Draham and Babouch, and the southern part, are associated with a high and very high level of susceptibility. These zones represent 30.89 (ANN) and 24.64 (AHP) of the study area. The zones designated as low to very low susceptibility are located in the north-eastern part of the study area, essentially in the Tabarka Plain. The area covered by these zones represents 40.97% (ANN) and 48.88% (APH) of the total area. The highest area was covered by the low to very low susceptible zone for both AHP and ANN.

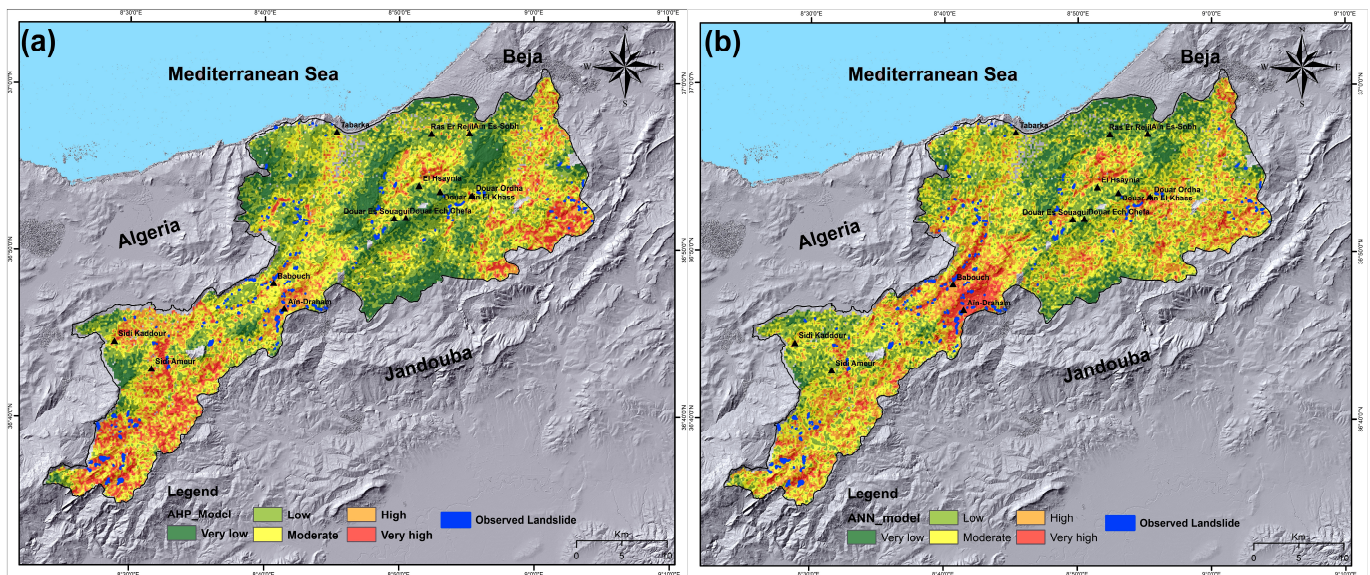


Figure 8. Susceptibility of landslide maps. (a) AHP model; (b) ANN model.

To assess these differences, a confusion matrix was employed to compare the three susceptible zones of the two models (Table 4)

Table 4. Confusion Matrix Comparing ANN and AHP Model Predictions Across Susceptibility Zones.

	AHP 1	AHP 2	AHP 3	Total
ANN 1	6374	1055	590	8019
ANN 2	3067	6111	2125	11,303
ANN 3	0	3501	2191	5692
Total	9441	10,667	4906	25,014

AHP 1: very low to low zone, AHP 2: moderate zone, AHP 3: high to very high zone, ANN 1: very low to low zone, ANN 2: moderate zone, ANN 3: high to very high zone.

This analysis reveals notable differences in performance across the three susceptibility zones. In the low to very Low zone, the ANN model demonstrated the strongest performance, achieving the highest precision (0.795), recall (0.675), and F1-score (0.730). These results suggest a strong alignment with the AHP model, indicating that the ANN model was highly effective in identifying instances within this zone. In contrast, the moderate zone demonstrated more balanced performance, with precision (0.541), recall (0.573), and F1-score (0.556). The high to very high zone demonstrated the least performance, with precision (0.446), recall (0.447), and F1-score (0.413).

To validate the computed models and to define the spatial distribution of the risk zone, the generated susceptibility models were overlaid by the known landslide obtained from the landslide inventory map.

The histogram method of the AHP susceptibility model (Figure 9a and Table 5) indicates that the highest number of observed landslides is associated with the high to very high susceptible area (39.27%). The second class corresponds to the moderately susceptible class with a percentage of 32.72%. 28% of the observed landslides in the field coincide with the region characterized by very low to low susceptibility.

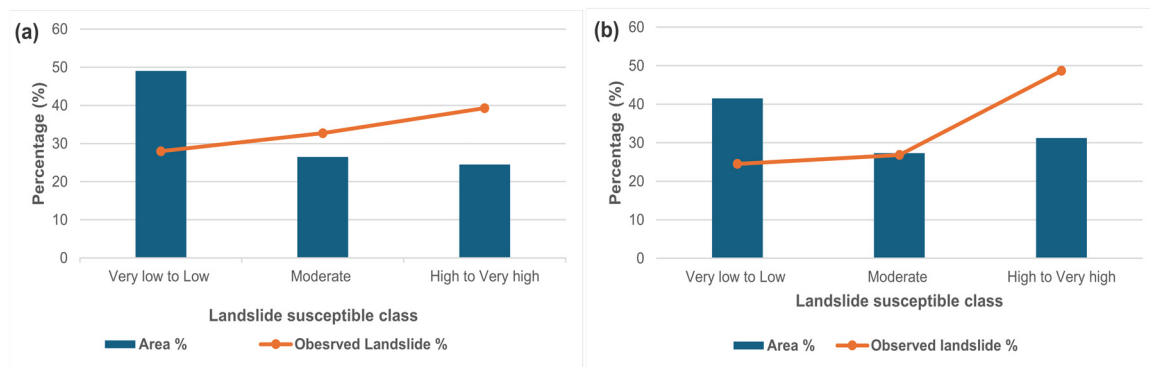


Figure 9. Susceptible areas histogram. (a) From the AHP model that falls into various classes, and (b) from the ANN model that falls into various classes.

Table 5. Landslide distribution in various landslide susceptible zones.

	Class	Area (%)	Observed Landslide (%)
AHP	Very low to Low	49.04	28.00
	Moderate	26.48	32.73
	High to Very high	24.48	39.27
ANN	Very low to Low	41.50	24.50
	Moderate	27.29	26.85
	High to Very high	31.22	48.66

For the ANN model (Figure 9b and Table 5), a total of 48.65% of the observed landslides are categorized as high to very high susceptibility. The category of moderate susceptibility is associated with 26.84% of the observed landslides. The class expressing the lowest level of susceptibility (very low to low) exhibits the lowest number of observed landslides (24.49%).

The performance of landslide susceptibility mapping can be evaluated using the ROC. The calculated area under the curve (AUC) is employed to evaluate the accuracy of the landslide susceptibility maps and reveals values corresponding to 0.651 and 0.720 for the AHP and ANN methods, respectively (Figure 10). These results show the efficiency of both methods applied, with an advantage of the ANN method attested by the highest AUC value (Figure 10).

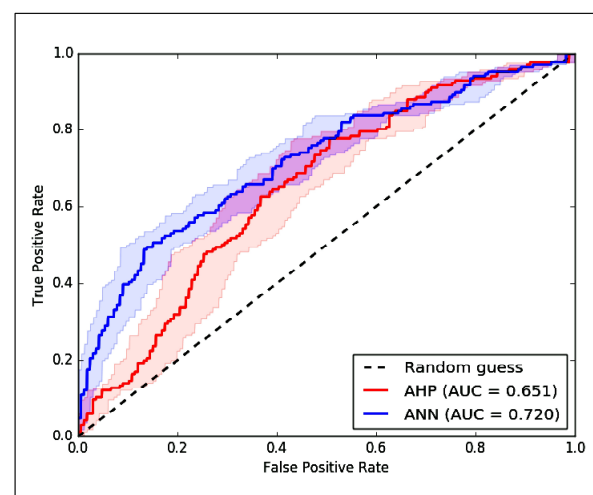


Figure 10. The ROC curve for both models of landslide susceptibility.

4. Discussion

The northwestern part of Tunisia has suffered from devastating landslides. Therefore, landslide susceptibility mapping is useful for identifying areas prone to landslides. It is essential for enhancing landslide prevention efforts and risk evaluation. Current research focuses on developing models of landslide susceptibility through the use of AHP and ANN approaches.

An inventory map integrating multiple data sources and covering 286 landslide locations mapped as polygons was realized. Ten landslide factors are selected according to the literature, the questionnaire survey, and the availability of data.

The key factors that influence landslide susceptibility in the current study were determined based on the weighting factor computed through the ANN and AHP (Table 2). The results enable the classification of the integrated factors, respectively, as follows: rainfall, slope, aspect, TRI, lithology, and LULC. Historical landslides, which are correlated with areas of high and very high susceptibility, coincide with regions that have steep slopes and heavy rainfall.

These areas are oriented towards the southeast and south and are characterized by extensive areas of bare soil and water. The high susceptibility areas are distinguished by a clayey lithology proving the role of clay properties in triggering landslides in the flysch massif made essentially by clay, silt, and sandstone of Ain Draham, northwestern Tunisia, as mentioned by the previous studies [90]. The areas characterized by a very low and low susceptibility are associated with a flat surface, receiving the least rainfall amount (970–1100 mm/y) and characterized by a gentle slope.

The results show that both AHP and ANN are able to produce accurate and reliable landslide susceptibility models. The efficiency of the applied method has been previously demonstrated in the literature [91].

The performance of the produced landslide susceptibility models is evaluated using the histogram of susceptibility area method and the ROC curve. In order to compare the distribution of susceptibility classes (very low to low, moderate, high to very high) between the two landslide models, the histogram method provides an effective approach. This comparison helps assess the delineation of risk areas by each model and the relative importance assigned to different susceptibility levels. Histogram analysis shows that the AHP model identifies 39.27% of the area with high to very high susceptibility, 32.72% with moderate susceptibility and 28% with very low to low susceptibility, whereas the ANN model indicates a larger area with high to very high susceptibility (48.65%), with moderate and very low to low susceptibility zones covering 26.84% and 24.49% of the area, respectively. This distribution reflects the two models' fundamental methodological differences. The histogram method demonstrates that the ANN model identifies a larger high-susceptibility area, which may indicate a more accurate approach to landslide susceptibility, while the AHP model provides a more uniform distribution across susceptibility classes.

The Analytic Hierarchy Process (AHP) is a multi-criteria decision-making approach that relies on expert judgment to assign weights to landslide factors. The AHP model generally produces a more accurate classification across susceptibility zones, with a proportional distribution between high, moderate, and low classes. This method is valued for its ability to provide clear and concise results, making it a valuable tool for decision-makers in GIS environments. However, AHP's use of subjective weighting can limit its predictive accuracy. In contrast, the ANN model is a data-driven machine learning approach capable of capturing complex nonlinear relationships among multiple factors influencing landslides. The higher proportion of high susceptibility zones in the ANN model suggests that the ANN is more accurate in identifying potentially high-risk areas, likely due to its ability to learn intricate patterns from the training data.

In the current study, ROC curve analysis was also employed to evaluate landslide susceptibility mapping, providing a reliable and quantitative comparison of the predictive performance of AHP and ANN models. The calculated area under the curve (AUC) values for the landslide susceptibility models are 0.651 and 0.720 for the ANN and AHP methods, respectively. The results indicate that the ANN method is more accurate than the AHP method. Our results are consistent with those of comparable comparative studies. In particular, the study by [92] presents a comprehensive landslide susceptibility analysis conducted on Jeju Island, South Korea. The analysis employed two methods, the Analytic Hierarchy Process (AHP) and Artificial Neural Network (ANN) integrated with GIS technology. The analysis utilized seven factors: slope, aspect, soil type, geological type, rainfall intensity, forest, and land cover. The study concluded that the ANN method was more appropriate than the AHP method. Moreover, ref. [93] focuses on the development of landslide susceptibility maps of Darjeeling Himalayas, West Bengal, India by integrating three advanced modeling approaches within a GIS environment: Artificial Neural Network (ANN), Fuzzy Analytical Hierarchy Process (Fuzzy-AHP), and Multi-Criteria Decision Analysis (MCDA). The aim of this study is to determine the most effective method for identifying the landslide-prone zone by comparing the performance of three different approaches. The methodology used ten input factors, namely Slope, aspect, profile curvature, drainage density, lineament density, geomorphology, soil texture, land use and land cover, lithology, and rainfall. The models were evaluated using the Area Under the Curve (AUC) of Receiver Operating Characteristic (ROC) curves to measure predictive accuracy. The ANN model showed slightly better predictive performance with an AUC of 88.1% compared to Fuzzy-AHP and MCDA, with AUC values of 86.1% and 85.4% for the Fuzzy-AHP model and the AHP model, respectively. In addition, the study [94] applied the Frequency ratio (Fr), Analytical hierarchy process (AHP), Logistic regression (LR), and Artificial Neural Network (ANN) models to assess landslide susceptibility in the Republic of Korea. Topographical, hydrogeological, soil, forest, and land cover factors were employed in the landslide susceptibility analysis. The ANN model exhibits the most accurate prediction with Area Under Curve (AUC) values around 0.806. It is slightly better than FR, AHP, and LR, with AUC values of 0.794, 0.784, and 0.794, respectively.

Studies show that machine learning models, including ANN, consistently outperform classical statistical methods in terms of accuracy and predictive capability, as measured by the Area Under the Receiver Operating Characteristic Curve (AUC).

5. Conclusions

The study region has experienced significant damage from calamitous landslides. Therefore, in order to create effective strategies for preventing landslides, the current research is focused on developing landslide susceptibility maps for the northwestern region of Tunisia. The AHP and ANN were utilized to achieve this. Firstly, an inventory map was performed; in this study, 286 landslide locations were mapped by field surveys, historical records, and data series from Google Earth. Then, landslide factors were carefully carried out, including rainfall, slope, aspect, TRI, lithology, LULC, distance from streams, drainage density, lineament density, and distance from roads. The rainfall and slope are of utmost significance among these factors. The evaluation of accuracy demonstrated that the ANN and AHP are the most appropriate models for producing maps of landslide susceptibility in the research area, by comparing the known landslide events and susceptible zones. Later, in order to determine the performance of the two approaches, we employed the area under the ROC curve (AUC). The AUC values of both models were acceptable. The ANN model showed superior outcomes overall, ranking above the AHP model. This research offers valuable resources for stakeholders, planners, and engineers, as it provides landslide

susceptibility maps. By taking appropriate preventive measures and mitigation procedures, they can make quick and well-informed decisions to reduce the damage resulting from current and future landslides and avoid the most vulnerable areas. Future efforts and model improvement should focus on additional factors such as LULC change over time, different geotechnical parameters, and geophysical data. Improved tools might be used to perform more accurate inventory maps, such as higher resolution Lidar data, and focus on the validation part, for instance, by using new techniques. Also, more advanced techniques such as deep learning could help produce more reliable landslide susceptibility results.

Author Contributions: Conceptualization, M.M. and D.S.; methodology, M.M. and D.S.; software, M.M.; validation, M.M., D.S., A.A., A.S., and H.-B.H.; formal analysis, M.M., D.S., A.A., and H.-B.H.; data curation, H.-B.H. and M.M.; writing—original draft preparation, M.M. and D.S.; writing—reviewing and editing, M.M., D.S., A.A., A.S., M.H.I., and H.-B.H.; visualization, M.M.; supervision, A.A., A.S., M.H.I., and H.-B.H. All authors have read and agreed to the published version of the manuscript.

Funding: This research received no external funding.

Data Availability Statement: Reports from the Ministry of Equipment's archives, the National Office of Mines (NOM), the Jandouba's Regional Commissariat for Agricultural Development, the German Aerospace Agency (DLR).

Acknowledgments: The authors acknowledge the German Aerospace Agency (DLR) for providing the TanDEM-X DEM data. The authors would like to express their sincere gratitude to the Editor and the anonymous reviewers for their thoughtful and constructive feedback on this manuscript.

Conflicts of Interest: The authors declare no conflicts of interest.

References

1. Pareek, N.; Sharma, M.L.; Arora, M.K. Impact of seismic factors on landslide susceptibility zonation: A case study in part of Indian Himalayas. *Landslides* **2010**, *7*, 191–201. [\[CrossRef\]](#)
2. Huang, Y.; Xu, C.; Zhang, X.; Li, L. Bibliometric analysis of landslide research based on the WOS database. *Nat. Hazards Res.* **2022**, *2*, 49–61. [\[CrossRef\]](#)
3. Saro, L.; Woo, J.S.; Kwan-Young, O.; Moun-Jin, L. The spatial prediction of landslide susceptibility applying artificial neural network and logistic regression models: A case study of Inje, Korea. *Open Geosci.* **2016**, *8*, 117–132. [\[CrossRef\]](#)
4. Moayedi, H.; Mehrabi, M.; Mosallanezhad, M.; Rashid, A.S.A.; Pradhan, B. Modification of landslide susceptibility mapping using optimized PSO-ANN technique. *Eng. Comput.* **2019**, *35*, 967–984. [\[CrossRef\]](#)
5. Kumar, M.; Krishnaveni, V.; Muthukumar, S. Geotechnical Investigation and Numerical Analysis of Slope Failure: A Case Study of Landslide Vulnerability Zone in Kolli Hills, Tamil Nadu. *J. Geol. Soc. India* **2021**, *97*, 513–519. [\[CrossRef\]](#)
6. Benchelha, S.; Aoudjehane, H.C.; Hakdaoui, M.; Hamdouni, R.E.; Mansouri, H.; Benchelha, T.; Layelmam, M.; Alaoui, M. Landslide susceptibility mapping in the municipality of oudka, northern morocco: A comparison between logistic regression and artificial neural networks models. *Int. Arch. Photogramm. Remote Sens. Spat. Inf. Sci.* **2019**, *42*, 41–49. [\[CrossRef\]](#)
7. Froude, M.J.; Petley, D.N. Global fatal landslide occurrence from 2004 to 2016. *Nat. Hazards Earth Syst. Sci.* **2018**, *18*, 2161–2181. [\[CrossRef\]](#)
8. Sim, K.B.; Lee, M.L.; Wong, S.Y. A review of landslide acceptable risk and tolerable risk. *Geoenviron. Disasters* **2022**, *9*, 3. [\[CrossRef\]](#)
9. Tiranti, D.; Cremonini, R. Editorial: Landslide Hazard in a Changing Environment. *Front. Earth Sci.* **2019**, *7*, 3. [\[CrossRef\]](#)
10. United Nations International Strategy for Disaster Reduction (UNISDR); United Nations Development Programme (UNDP). *City Profile, Progress and Action Plan—Case of Ain Drahem*; United Nations International Strategy for Disaster Reduction: Geneva, Switzerland; United Nations Development Programme: New York, NY, USA, 2015; p. 23.
11. Nohani, E.; Moharrami, M.; Sharafi, S.; Khosravi, K.; Pradhan, B.; Pham, B.T.; Lee, S.; Melesse, M.A. Landslide Susceptibility Mapping Using Different GIS-Based Bivariate Models. *Water* **2019**, *11*, 1402. [\[CrossRef\]](#)
12. Aldiansyah, S.; Wardani, F. Assessment of resampling methods on performance of landslide susceptibility predictions using machine learning in Kendari City, Indonesia. *Water Pract. Technol.* **2024**, *19*, 52–81. [\[CrossRef\]](#)
13. El Jazouli, A.; Barakat, A.; Khellouk, R. GIS-multicriteria evaluation using AHP for landslide susceptibility mapping in Oum Er Rbia high basin (Morocco). *Geoenviron. Disasters* **2019**, *6*, 3. [\[CrossRef\]](#)

14. Sonker, I.; Tripathi, J.N.; Singh, A.K. Landslide susceptibility zonation using geospatial technique and analytical hierarchy process in Sikkim Himalaya. *Quat. Sci. Adv.* **2021**, *4*, 100039. [\[CrossRef\]](#)
15. Liu, X.; Shao, S.; Shao, S. Landslide susceptibility zonation using the analytical hierarchy process (AHP) in the Great Xi'an Region, China. *Sci. Rep.* **2024**, *14*, 2941. [\[CrossRef\]](#) [\[PubMed\]](#)
16. Thapa, D.; Bhandari, B.P. GIS-Based Frequency Ratio Method for Identification of Potential Landslide Susceptible Area in the Siwalik Zone of Chatara-Barahakshetra Section, Nepal. *Open J. Geol.* **2019**, *9*, 873–896. [\[CrossRef\]](#)
17. Youssef, B.; Bouskri, I.; Brahim, B.; Kader, S.; Brahim, I.; Abdelkrim, B.; Spalević, V. The contribution of the frequency ratio model and the prediction rate for the analysis of landslide risk in the Tizi N'tichka area on the national road (RN9) linking Marrakech and Ouarzazate. *Catena* **2023**, *232*, 107464. [\[CrossRef\]](#)
18. Al-Najjar, H.A.H.; Pradhan, B. Spatial landslide susceptibility assessment using machine learning techniques assisted by additional data created with generative adversarial networks. *Geosci. Front.* **2021**, *12*, 625–637. [\[CrossRef\]](#)
19. Huang, J.; Zeng, X.; Ding, L.; Yin, Y.; Li, Y. Landslide Susceptibility Evaluation Using Different Slope Units Based on BP Neural Network. *Comput. Intell. Neurosci.* **2022**, *2022*, 9923775. [\[CrossRef\]](#) [\[PubMed\]](#)
20. Shahabi, H.; Ahmadi, R.; Alizadeh, M.; Hashim, M.; Al-Ansari, N.; Shirzadi, A.; Wolf, I.D.; Ariffin, E.H. Landslide Susceptibility Mapping in a Mountainous Area Using Machine Learning Algorithms. *Remote Sens.* **2023**, *15*, 3112. [\[CrossRef\]](#)
21. Lee, D.-H.; Kim, Y.-T.; Lee, S.-R. Shallow Landslide Susceptibility Models Based on Artificial Neural Networks Considering the Factor Selection Method and Various Non-Linear Activation Functions. *Remote Sens.* **2020**, *12*, 1194. [\[CrossRef\]](#)
22. Selamat, S.N.; Majid, N.A.; Taha, M.R.; Osman, A. Landslide Susceptibility Model Using Artificial Neural Network (ANN) Approach in Langat River Basin, Selangor, Malaysia. *Land* **2022**, *11*, 833. [\[CrossRef\]](#)
23. Jennifer, J.J.; Saravanan, S. Artificial neural network and sensitivity analysis in the landslide susceptibility mapping of Idukki district, India. *Geocarto Int.* **2022**, *37*, 5693–5715. [\[CrossRef\]](#)
24. Tien Bui, D.; Ho, T.C.; Revhaug, I.; Pradhan, B.; Nguyen, D.B. Landslide Susceptibility Mapping Along the National Road 32 of Vietnam Using GIS-Based J48 Decision Tree Classifier and Its Ensembles. In *Cartography from Pole to Pole*; Buchroithner, M., Prechtel, N., Burghardt, D., Eds.; Lecture Notes in Geoinformation and Cartography; Springer: Berlin/Heidelberg, Germany, 2014; pp. 303–317, ISBN 978-3-642-32617-2.
25. Park, S.-J.; Lee, C.-W.; Lee, S.; Lee, M.-J. Landslide Susceptibility Mapping and Comparison Using Decision Tree Models: A Case Study of Jumunjin Area, Korea. *Remote Sens.* **2018**, *10*, 1545. [\[CrossRef\]](#)
26. Lee, S.; Hong, S.-M.; Jung, H.-S. A Support Vector Machine for Landslide Susceptibility Mapping in Gangwon Province, Korea. *Sustainability* **2017**, *9*, 48. [\[CrossRef\]](#)
27. Huang, Y.; Zhao, L. Review on landslide susceptibility mapping using support vector machines. *Catena* **2018**, *165*, 520–529. [\[CrossRef\]](#)
28. Akinci, H.; Kilicoglu, C.; Dogan, S. Random Forest-Based Landslide Susceptibility Mapping in Coastal Regions of Artvin, Turkey. *ISPRS Int. J. Geo-Inf.* **2020**, *9*, 553. [\[CrossRef\]](#)
29. Riestu, I.; Hidayat, H. Landslide Susceptibility Mapping Using Random Forest Algorithm and Its Correlation With Land Use In Batu City, Jawa Timur. *IOP Conf. Ser. Earth Environ. Sci.* **2023**, *1127*, 12017. [\[CrossRef\]](#)
30. Ghorbanzadeh, O.; Rostamzadeh, H.; Blaschke, T.; Gholaminia, K.; Aryal, J. A new GIS-based data mining technique using an adaptive neuro-fuzzy inference system (ANFIS) and k-fold cross-validation approach for land subsidence susceptibility mapping. *Nat. Hazards* **2018**, *94*, 497–517. [\[CrossRef\]](#)
31. Mehrabi, M.; Pradhan, B.; Moayedi, H.; Alamri, A. Optimizing an Adaptive Neuro-Fuzzy Inference System for Spatial Prediction of Landslide Susceptibility Using Four State-of-the-art Metaheuristic Techniques. *Sensors* **2020**, *20*, 1723. [\[CrossRef\]](#) [\[PubMed\]](#)
32. Sun, X.; Chen, J.; Bao, Y.; Han, X.; Zhan, J.; Peng, W. Landslide Susceptibility Mapping Using Logistic Regression Analysis along the Jinsha River and Its Tributaries Close to Derong and Deqin County, Southwestern China. *ISPRS Int. J. Geo. Inf.* **2018**, *7*, 438. [\[CrossRef\]](#)
33. Puente-Sotomayor, F.; Mustafa, A.; Teller, J. Landslide Susceptibility Mapping of Urban Areas: Logistic Regression and Sensitivity Analysis applied to Quito, Ecuador. *Geoenviron. Disasters* **2021**, *8*, 19. [\[CrossRef\]](#)
34. Youssef, A.M.; Pourghasemi, H.R.; Pourtaghi, Z.S.; Al-Katheeri, M.M. Landslide susceptibility mapping using random forest, boosted regression tree, classification and regression tree, and general linear models and comparison of their performance at Wadi Tayyah Basin, Asir Region, Saudi Arabia. *Landslides* **2016**, *13*, 839–856. [\[CrossRef\]](#)
35. Chen, W.; Xie, X.; Peng, J.; Wang, J.; Duan, Z.; Hong, H. GIS-based landslide susceptibility modelling: A comparative assessment of kernel logistic regression, Naïve-Bayes tree, and alternating decision tree models. *Geomat. Nat. Hazards Risk* **2017**, *8*, 950–973. [\[CrossRef\]](#)
36. Bueechi, E.; Klimeš, J.; Frey, H.; Huggel, C.; Strozzi, T.; Cochachin, A. Regional-scale landslide susceptibility modelling in the Cordillera Blanca, Peru—A comparison of different approaches. *Landslides* **2019**, *16*, 395–407. [\[CrossRef\]](#)
37. Anis, Z.; Wissem, G.; Vali, V.; Smida, H.; Mohamed Essghaier, G. GIS-based landslide susceptibility mapping using bivariate statistical methods in North-western Tunisia. *Open Geosci.* **2019**, *11*, 708–726. [\[CrossRef\]](#)

38. Klai, A.; Haddad, R.; Bouzid, M.K.; Rabia, M.C. Landslide susceptibility mapping by fuzzy gamma operator and GIS, a case study of a section of the national road n°11 linking Mateur to Béja (Northwestern Tunisia). *Arab. J. Geosci.* **2020**, *13*, 58. [\[CrossRef\]](#)
39. Mansour, R.; Zouaoui, N.; El Ghali, A. Quantitative assessment of landslide risk in northwestern Tunisia using probabilistic approaches. *Arab. J. Geosci.* **2022**, *15*, 1608. [\[CrossRef\]](#)
40. Klai, A.; Katlane, R.; Haddad, R.; Rabia, M.C. Landslide susceptibility mapping by frequency ratio and fuzzy logic approach: A case study of Mogods and Hedil (Northern Tunisia). *Appl. Geomat.* **2024**, *16*, 91–109. [\[CrossRef\]](#)
41. Wessel, B.; Huber, M.; Wohlfart, C.; Marschalk, U.; Kosmann, D.; Roth, A. Accuracy assessment of the global TanDEM-X Digital Elevation Model with GPS data. *ISPRS J. Photogramm. Remote Sens.* **2018**, *139*, 171–182. [\[CrossRef\]](#)
42. Mahalingam, R.; Olsen, M.J. Evaluation of the influence of source and spatial resolution of DEMs on derivative products used in landslide mapping. *Geomat. Nat. Hazards Risk* **2016**, *7*, 1835–1855. [\[CrossRef\]](#)
43. Brock, J.; Schratz, P.; Petschko, H.; Muenchow, J.; Micu, M.; Brenning, A. The performance of landslide susceptibility models critically depends on the quality of digital elevation models. *Geomat. Nat. Hazards Risk* **2020**, *11*, 1075–1092. [\[CrossRef\]](#)
44. Rouvier, H. Géologie de l'Extrême-Nord Tunisien: Tectoniques et Paléogéographies Superposées à l'Extrémité Orientale de la Chaîne Nord-Maghrébine. Ph.D. Thesis, University of Paris VI, Paris, France, 1977.
45. Ali, S.A.; Parvin, F.; Vojteková, J.; Costache, R.; Linh, N.T.T.; Pham, Q.B.; Vojtek, M.; Gigović, L.; Ahmad, A.; Ghorbani, M.A. GIS-based landslide susceptibility modeling: A comparison between fuzzy multi-criteria and machine learning algorithms. *Geosci. Front.* **2021**, *12*, 857–876. [\[CrossRef\]](#)
46. Dahim, M.; Alqadhi, S.; Mallick, J. Enhancing landslide management with hyper-tuned machine learning and deep learning models: Predicting susceptibility and analyzing sensitivity and uncertainty. *Front. Ecol. Evol.* **2023**, *11*, 1108924. [\[CrossRef\]](#)
47. Wang, F.; Xu, P.; Wang, C.; Wang, N.; Jiang, N. Application of a GIS-Based Slope Unit Method for Landslide Susceptibility Mapping along the Longzi River, Southeastern Tibetan Plateau, China. *ISPRS Int. J. Geo-Inf.* **2017**, *6*, 172. [\[CrossRef\]](#)
48. Wang, H.; Zhang, Y.C.; Hu, H.Y. A Study on Relationship of Landslide Occurrence and Rainfall. *Appl. Mech. Mater.* **2013**, 438–439, 1200–1204. [\[CrossRef\]](#)
49. Lee, M.-J. Rainfall and Landslide Correlation Analysis and Prediction of Future Rainfall Base on Climate Change. In *Geohazards Caused by Human Activity*; Farid, A., Ed.; InTechOpen: London, UK, 2016; ISBN 978-953-51-2801-4.
50. Silalahi, F.E.S.; Pamela; Arifianti, Y.; Hidayat, F. Landslide susceptibility assessment using frequency ratio model in Bogor, West Java, Indonesia. *Geosci. Lett.* **2019**, *6*, 10. [\[CrossRef\]](#)
51. Nakileza, B.R.; Nedala, S. Topographic influence on landslides characteristics and implication for risk management in upper Manafwa catchment, Mt Elgon Uganda. *Geoenviron. Disasters* **2020**, *7*, 27. [\[CrossRef\]](#)
52. Meten, M.; PrakashBhandary, N.; Yatabe, R. Effect of Landslide Factor Combinations on the Prediction Accuracy of Landslide Susceptibility Maps in the Blue Nile Gorge of Central Ethiopia. *Geoenviron. Disasters* **2015**, *2*, 9. [\[CrossRef\]](#)
53. Achour, Y.; Boumezbeur, A.; Hadji, R.; Chouabbi, A.; Cavaleiro, V.; Bendaoud, E.A. Landslide susceptibility mapping using analytic hierarchy process and information value methods along a highway road section in Constantine, Algeria. *Arab. J. Geosci.* **2017**, *10*, 194. [\[CrossRef\]](#)
54. Celtek, S. The Effect of Aspect on Landslide and Its Relationship with Other Parameters. In *Landslides*; Zhang, Y., Cheng, Q., Eds.; IntechOpen: London, UK, 2022; ISBN 978-1-83969-023-5.
55. Kornejady, A.; Ownegh, M.; Bahremand, A. Landslide susceptibility assessment using maximum entropy model with two different data sampling methods. *Catena* **2017**, *152*, 144–162. [\[CrossRef\]](#)
56. Kalantar, B.; Pradhan, B.; Naghibi, S.A.; Motevalli, A.; Mansor, S. Assessment of the effects of training data selection on the landslide susceptibility mapping: A comparison between support vector machine (SVM), logistic regression (LR) and artificial neural networks (ANN). *Geomat. Nat. Hazards Risk* **2018**, *9*, 49–69. [\[CrossRef\]](#)
57. Pawluszek, K.; Borkowski, A. Impact of DEM-derived factors and analytical hierarchy process on landslide susceptibility mapping in the region of Rożnów Lake, Poland. *Nat. Hazards* **2017**, *86*, 919–952. [\[CrossRef\]](#)
58. Regmi, N.R.; Walter, J.I. Detailed mapping of shallow landslides in eastern Oklahoma and western Arkansas and potential triggering by Oklahoma earthquakes. *Geomorphology* **2020**, *366*, 106806. [\[CrossRef\]](#)
59. Wubalem, A. Landslide Inventory, Susceptibility, Hazard and Risk Mapping. In *Landslides*; Zhang, Y., Cheng, Q., Eds.; IntechOpen: London, UK, 2022; ISBN 978-1-83969-023-5.
60. Trisnawati, D.; Najib; Hidayatillah, A.S. The Relationship of Lithology with Landslide Occurrences in Banyumanik and Tembalang Districts, Semarang City. *IOP Conf. Ser. Earth Environ. Sci.* **2022**, *1047*, 012026. [\[CrossRef\]](#)
61. Dehnavi, A.; Aghdam, I.N.; Pradhan, B.; Morshed Varzandeh, M.H. A new hybrid model using step-wise weight assessment ratio analysis (SWARA) technique and adaptive neuro-fuzzy inference system (ANFIS) for regional landslide hazard assessment in Iran. *Catena* **2015**, *135*, 122–148. [\[CrossRef\]](#)
62. Bourenane, H.; Guettouche, M.S.; Bouhadad, Y.; Braham, M. Landslide hazard mapping in the Constantine city, Northeast Algeria using frequency ratio, weighting factor, logistic regression, weights of evidence, and analytical hierarchy process methods. *Arab. J. Geosci.* **2016**, *9*, 154. [\[CrossRef\]](#)

63. Shafique, M.; Van Der Meijde, M.; Khan, M.A. A review of the 2005 Kashmir earthquake-induced landslides; from a remote sensing prospective. *J. Asian Earth Sci.* **2016**, *118*, 68–80. [\[CrossRef\]](#)
64. Masruroh, H.; Leksono, A.S.; Kurniawan, S.; Soemarno, S. Developing landslide susceptibility map using Artificial Neural Network (ANN) method for mitigation of land degradation. *J. Degrad. Min. Land Manage.* **2023**, *10*, 4479. [\[CrossRef\]](#)
65. Çellek, S. Effect of Stream Distance on Landslide. In Proceedings of the SETSCI Conference Proceedings, 3rd International Symposium on Innovative Approaches in Scientific Studies (Engineering and Natural Sciences) (ISAS2019-ENS), Ankara, Turkey, 19 April 2019; pp. 268–275.
66. Tadesse, L.; Uncha, A.; Toma, T. Landslide vulnerability mapping using multi-criteria decision-making approaches: In Gacho Babba District, Gamo Highlands Southern Ethiopia. *Discov. Appl. Sci.* **2024**, *6*, 31. [\[CrossRef\]](#)
67. Budimir, M.E.A.; Atkinson, P.M.; Lewis, H.G. A systematic review of landslide probability mapping using logistic regression. *Landslides* **2015**, *12*, 419–436. [\[CrossRef\]](#)
68. Kumar, A.; Sharma, R.K.; Bansal, V.K. Landslide hazard zonation using analytical hierarchy process along National Highway-3 in mid Himalayas of Himachal Pradesh, India. *Env. Earth Sci.* **2018**, *77*, 719. [\[CrossRef\]](#)
69. Yamusa, B.I.; Ismail, S.M. Integration of lineament and strain analysis to assess landslide vulnerability along taiping to Ipoh Highway, Malaysia. *Int. Arch. Photogramm. Remote Sens. Spat. Inf. Sci.* **2023**, *48*, 57–74. [\[CrossRef\]](#)
70. Zhao, P.; Masoumi, Z.; Kalantari, M.; Aflaki, M.; Mansourian, A. A GIS-Based Landslide Susceptibility Mapping and Variable Importance Analysis Using Artificial Intelligent Training-Based Methods. *Remote Sens.* **2022**, *14*, 211. [\[CrossRef\]](#)
71. Zhao, Y.; Wang, R.; Jiang, Y.; Liu, H.; Wei, Z. GIS-based logistic regression for rainfall-induced landslide susceptibility mapping under different grid sizes in Yueqing, Southeastern China. *Eng. Geol.* **2019**, *259*, 105147. [\[CrossRef\]](#)
72. Khalil, U.; Imtiaz, I.; Aslam, B.; Ullah, I.; Tariq, A.; Qin, S. Comparative analysis of machine learning and multi-criteria decision making techniques for landslide susceptibility mapping of Muzaffarabad district. *Front. Environ. Sci.* **2022**, *10*, 1028373. [\[CrossRef\]](#)
73. Khan, Z.; Nawazuzzoha, M.; Abdelrahman, K.; Ali, S.A.; Fnais, M.S.; Kausar Shamim, S.; Ahmad, A.; András, P. Mapping landslide susceptibility and risk assessment on fragile ecosystem of Himalayan River basins. *All Earth* **2025**, *37*, 1–22. [\[CrossRef\]](#)
74. Liu, X.; Shao, S.; Zhang, C.; Shao, S. Landslide susceptibility prediction in the loess tableland considering geomorphic evolution. *Catena* **2025**, *249*, 108668. [\[CrossRef\]](#)
75. Semih, T.; Seyhan, S. A multi-criteria factor evaluation model for gas station site selection. *J. Glob. Manag.* **2011**, *2*, 12–21.
76. Saaty, T.L. How to make a decision: The Analytic Hierarchy Process. *Eur. J. Oper. Res.* **1990**, *48*, 9–26. [\[CrossRef\]](#)
77. Saaty, T.L. *The Analytic Hierarchy Process: Planning, Priority Setting, Resource Allocation*; MacGraw-Hill: New York, NY, USA, 1980; p. 287.
78. Saaty, T.L.; Vargas, L.G. The possibility of group choice: Pairwise comparisons and merging functions. *Soc. Choice Welf.* **2012**, *38*, 481–496. [\[CrossRef\]](#)
79. Chen, Y.; Liu, R.; Barrett, D.; Gao, L.; Zhou, M.; Renzullo, L.; Emelyanova, I. A spatial assessment framework for evaluating flood risk under extreme climates. *Sci. Total Environ.* **2015**, *538*, 512–523. [\[CrossRef\]](#) [\[PubMed\]](#)
80. Souissi, D.; Souie, A.; Sebei, A.; Mahfoudhi, R.; Zghibi, A.; Zouhri, L.; Amiri, W.; Ghanmi, M. Flood hazard mapping and assessment using fuzzy analytic hierarchy process and GIS techniques in Takelsa, Northeast Tunisia. *Arab. J. Geosci.* **2022**, *15*, 1405. [\[CrossRef\]](#)
81. Souissi, D.; Zouhri, L.; Hammami, S.; Msaddek, M.H.; Zghibi, A.; Dlala, M. GIS-based MCDM–AHP modeling for flood susceptibility mapping of arid areas, southeastern Tunisia. *Geocarto Int.* **2020**, *35*, 991–1017. [\[CrossRef\]](#)
82. Lee, S.; Ryu, J.; Min, K.; Won, J. Landslide susceptibility analysis using GIS and artificial neural network. *Earth Surf. Process. Landf.* **2003**, *28*, 1361–1376. [\[CrossRef\]](#)
83. Merghadi, A.; Yunus, A.P.; Dou, J.; Whiteley, J.; ThaiPham, B.; Bui, D.T.; Avtar, R.; Abderrahmane, B. Machine learning methods for landslide susceptibility studies: A comparative overview of algorithm performance. *Earth Sci. Rev.* **2020**, *207*, 103225. [\[CrossRef\]](#)
84. Riedmiller, M.; Braun, H. A direct adaptive method for faster backpropagation learning: The RPROP algorithm. In Proceedings of the IEEE International Conference on Neural Networks, San Francisco, CA, USA, 28 March–1 April 1993; pp. 586–591.
85. Fritsch, S.; Günther, F.; Wright, M. Neuralnet: Training of Neural Networks; R Package Version 1.44.2; 2019. Available online: <https://cran.r-project.org/web/packages/neuralnet/index.html> (accessed on 30 November 2021).
86. Gholami, M.; Ghachkanlu, E.N.; Khosravi, K.; Pirasteh, S. Landslide prediction capability by comparison of frequency ratio, fuzzy gamma and landslide index method. *J. Earth Syst. Sci.* **2019**, *128*, 42. [\[CrossRef\]](#)
87. Yong, C.; Jinlong, D.; Fei, G.; Bin, T.; Tao, Z.; Hao, F.; Li, W.; Qinghua, Z. Review of landslide susceptibility assessment based on knowledge mapping. *Stoch. Environ. Res. Risk Assess.* **2022**, *36*, 2399–2417. [\[CrossRef\]](#)
88. Bathrellos, G.D.; Koukouvelas, I.K.; Skilodimou, H.D.; Nikolakopoulos, K.G.; Vgenopoulos, A.-L. Landslide causative factors evaluation using GIS in the tectonically active Glafkos River area, northwestern Peloponnese, Greece. *Geomorphology* **2024**, *461*, 109285. [\[CrossRef\]](#)

89. Vakhshoori, V.; Zare, M. Is the ROC curve a reliable tool to compare the validity of landslide susceptibility maps? *Geomat. Nat. Hazards Risk* **2018**, *9*, 249–266. [[CrossRef](#)]
90. Anis, Z.; Wissem, G.; Riheb, H.; Biswajeet, P.; Mohamed Essghaier, G. Effects of clay properties in the landslides genesis in flysch massif: Case study of Ain Drahem, North Western Tunisia. *J. Afr. Earth Sci.* **2019**, *151*, 146–152. [[CrossRef](#)]
91. Salleh, S.A.; Abd Rahman, A.S.A.; Othman, A.N.; Wan Mohd, W.M.N. Comparative study of landslides susceptibility mapping methods: Multi-Criteria Decision Making (MCDM) and Artificial Neural Network (ANN). *IOP Conf. Ser. Earth Environ. Sci.* **2018**, *117*, 12035. [[CrossRef](#)]
92. Quan, H.-C.; Lee, B.-G. GIS-based landslide susceptibility mapping using analytic hierarchy process and artificial neural network in Jeju (Korea). *KSCE J. Civ. Eng.* **2012**, *16*, 1258–1266. [[CrossRef](#)]
93. Saha, A.; Villuri, V.G.K.; Bhardwaj, A. Development and Assessment of GIS-Based Landslide Susceptibility Mapping Models Using ANN, Fuzzy-AHP, and MCDA in Darjeeling Himalayas, West Bengal, India. *Land* **2022**, *11*, 1711. [[CrossRef](#)]
94. Young, O.C.; Cheung, K.; Choi, C.U. The Comparative Research of Landslide Susceptibility Mapping Using FR, AHP, LR, ANN. In Proceedings of the proceedings.esri.com, 2003. Available online: https://scholar.google.com/scholar?cluster=12686636575347739558&hl=fr&as_sdt=0,5 (accessed on 20 June 2024).

Disclaimer/Publisher’s Note: The statements, opinions and data contained in all publications are solely those of the individual author(s) and contributor(s) and not of MDPI and/or the editor(s). MDPI and/or the editor(s) disclaim responsibility for any injury to people or property resulting from any ideas, methods, instructions or products referred to in the content.